Soil & Tillage Research 145 (2015) 157–170

Contents lists available at ScienceDirect

Soil & Tillage Research

journal homepage: www.elsevier.com/locate/still

Finite element simulation of soil failure patterns under soil bin and field testing conditions

A.A. Tagar [a,b], Ji Changying [a,*], Jan Adamowski [c], Julien Malard [c], Chen Shi Qi [a], Ding Qishuo [a], N.A. Abbasi [c]

[a] College of Engineering, Nanjing Agricultural University, Nanjing 210031, PR China
[b] Faculty of Agricultural Engineering, Sindh Agriculture University, Tandojam 70060, Pakistan
[c] Department of Bioresource Engineering, McGill University, Sainte-Anne-de-Bellevue, Quebec H9X3V9, Canada

ARTICLE INFO

Article history:
Received 5 December 2013
Received in revised form 30 August 2014
Accepted 1 September 2014

Keywords:
Consistency limits
Finite element method
Sticky point
Soil physical and mechanical properties
Paddy soil

ABSTRACT

Finite element modeling (FEM) of soil physical behavior can provide information which is difficult or impossible to obtain experimentally. This method has been applied by many researchers to study soil compaction, acting forces on tools, stress distribution in soils and soil failure patterns. The great majority of studies that have investigated soil failure patterns have been limited to in-laboratory soil bins, with few tests being done under field conditions. However, it is difficult to simulate actual soil conditions in a soil bin. This study used FEM for the simulation of the soil failure patterns as linked to consistency limits and sticky point of soil, comparing the simulation results with soil failure patterns observed in the soil bin and in the field. Results showed that FEM is a useful tool to simulate soil failure patterns; however, simulation models correlated better with soil bin than with field test results. The results also showed the presence of a direct relationship between soil failure patterns and the consistency limits of the soil, both in the soil bin and in the field. However, soil bin results were not satisfactorily verified in the field, in particular as the failure patterns were also found to be affected by the roots of the stubbles in the field. It is concluded that FEM can provide accurate simulation of soil failure patterns under soil bin test conditions, but that soil bin results did not satisfactorily represent results from the field.

1. Introduction

Numerical methods are helpful in understanding and describing soil cutting processes and soil–tool interactions. Karmakar and Kushwaha (2006) identified three numerical methods to model the soil cutting process, namely the finite element method (FEM), the discrete element method (DEM) and computational fluid dynamics (CFD). The discrete element method (DEM) is based on a promising approach for constructing a high-fidelity model to describe the soil-tillage tool interaction (Shmulevich, 2010). However, the determination of model parameters to control the soil void ratio and the shape of particles, as well as the modeling of breakage and the formation of aggregates of varying sizes and shapes, remain significant challenges and limit the application of DEM for practical engineering problems (Abo Al-Kheer et al., 2011b). Computational fluid dynamics (CFD) can be used to model soil–tool interactions (Karmakar and Kushwaha, 2006). Soil dynamic behavior using the CFD simulation will help in tool design and its optimization with different shapes in order to reduce tool draft and energy demand over a wide speed range, and help model different types of soils based on their visco-plastic parameters. However, further research is needed before CFD can be used to model soil–tool interactions with confidence (Coetzee and Els, 2009). On the other hand, the finite element method (FEM) has been used by many researchers in order to design tillage tools and to investigate the interaction between soil and tillage implements. FEM can be used to study soil compaction, acting forces on tools, stress distribution in soil and soil failure patterns (Raper and Erbach, 1990; Aluko and Chandler, 2004; Shahab Davoudi et al., 2008); however the continuity assumption in FEM does not allow crack propagation in soil (Jafari et al., 2006). Coleman and Perumpral (1974) pointed out that in soil mechanics research, the FEM method is capable of providing information which is difficult or impossible to obtain experimentally. Later, Yong and Hanna (1977) modeled soil cutting by simple plane (two-dimensional) blades, and Liu Yan and HouZhi-Min (1985) and Chi and Kushwaha (1987, 1989) applied FEM to the study of three-dimensional soil cutting with narrow blades. FEM is also appropriate for the analysis of soil cutting problems where shear failure with significant plastic deformation occurs (Aluko, 2008).

* Corresponding author. Tel.: +86 13914706344.
E-mail address: ahmed_ali_tagar@hotmail.com (A.A. Tagar).

http://dx.doi.org/10.1016/j.still.2014.09.006

The performance of agricultural implements and the resulting soil tilth depend largely on the mechanical behavior of soils (Rajaram and Erbach, 1998). Soil failure patterns are one of the most important indices to assess the mechanical behavior of soils under varied soil and tool conditions. Indeed, Abo Al-Kheer et al., (2011a) concluded that the variation in soil failure patterns can be attributed to the wide variations in mechanical behavior of the soil. Previous studies of soil cutting have identified six types of soil failure patterns, namely collapse, brittle, chip-forming, bending, flow and flow with considerable bending in different soil types (Elijah and Weber, 1971; Rajaram and Gee-Clough, 1988; Rajaram and Erbach, 1996; Tagar et al., 2014). Collapse failure, which occurs in dry soils, involves the collapse of soil structure when a mass of a soil in front of the tool is crushed (Rajaram, 1990) and is similar to the shear plane-type failure as described by Elijah and Weber (1971). Brittle failure occurs in moist soils due to the propagation of tensile cracks (Chandler, 1984; Hatibu, 1987). Chip-forming failure, or plastic type failure, occurs in wet unsaturated soil conditions when the soil is removed in the form of chips similar to the chips formed in metal cutting (Rajaram and Erbach, 1996; Rajaram and Gee-Clough, 1988). Flow failure occurs in wet saturated soil conditions due to the mere physical displacement of the soil (Rajaram and Erbach, 1996), and bending failure is similar to flow failure but also shows some strain in the vertical direction (Elijah and Weber, 1971). Flow with considerable bending failure occurs at the sticky point of soil and is similar to flow failure but with considerable bending and no strains of elements (Tagar et al., 2014).

Rajaram and Erbach (1996, 1998) concluded that, to better understand tillage, research should be directed towards explaining various soil failure patterns and the resulting physical property changes. Indeed, Mamman and Oni (2005) carried out a study to investigate the effect of draught on the performance of model chisel furrowers. They concluded that there were no optimum values of tool speed or tillage depth for which the draught of the model tools were at a minimum. Therefore they suggested that the choice of model tool should depend on soil failure pattern at shallow depths, as well as on the size and quality of furrows created at deeper depths. Numerous studies have been conducted on soil failure patterns (e.g., Elijah and Weber, 1971; Stafford 1979a; Rajaram and Gee-Clough, 1988; Wang and Gee-Clough, 1993; Rajaram and Erbach, 1997, 1998, 1999; Aluko and Seig, 2000; Makanga et al., 2010); however, despite this large number of studies, a thorough understanding of soil failure patterns has not yet been achieved.

Of the large number of studies having investigated soil failure patterns, the vast majority have been limited to in-laboratory soil bins, with only a few tests being done under field conditions (e.g., Elijah and Weber, 1971; Hemmat et al., 2012). The justifications for soil bin studies include: better control of soil physical parameters (Stafford, 1979b) and the setting of operation variables (Wegscheid and Myers, 1967), as well as the possibility of replicating tests over short periods, independent of weather (Barnes and Bockhop, 1960). However, it is difficult to simulate actual soil conditions in a soil bin. This is consistent with Dexter and Bird (2001), who concluded that the properties of disturbed (remolded) soil are not appropriate for the prediction of the behavior of undisturbed soil in the field. Therefore, the verification of soil bin and laboratory experiments under realistic field conditions is always necessary (McKyes and Desir, 1984). This is consistent with Liu et al. (2007), who compared soil bin and field experimental soils. Overall, while soil bin study results may be extrapolated to the field scale, a great deal of caution must be taken, given the far greater soil heterogeneity at the field scale.

Although the importance of a better understanding of the true failure patterns of soils has been emphasized by a number of authors (e.g., Rajaram and Erbach, 1997, 1998; Mamman and Oni, 2005), the technical methods available to quantify soil failure patterns are limited. For instance, Jayasuriya and Salokhe (2001) concluded that the numerical value of the moisture content does not show any direct relationship with changes in soil failure patterns in different soils. Soil consistency limits could therefore be hypothesized to show a much clearer relationship with soil failure patterns than the simple numerical value of the moisture content, though this has not been previously studied in great detail. Although the study by Stafford (1979a) did indeed report the plastic and liquid limits of the experimental soils, the experimental soil moisture levels employed for testing unfortunately did not correspond to any of these limits.

Thus, the authors of this paper carried out a previous study to investigate soil failure patterns and draft as influenced by the consistency limits of the soil, and the results confirmed that there does exist a direct relationship between these variables (see Tagar et al., 2014). However, it is most important to verify the results in realistic field conditions. To date, most studies have focused on the simulation of soil stresses, soil forces, soil deformation, and soil

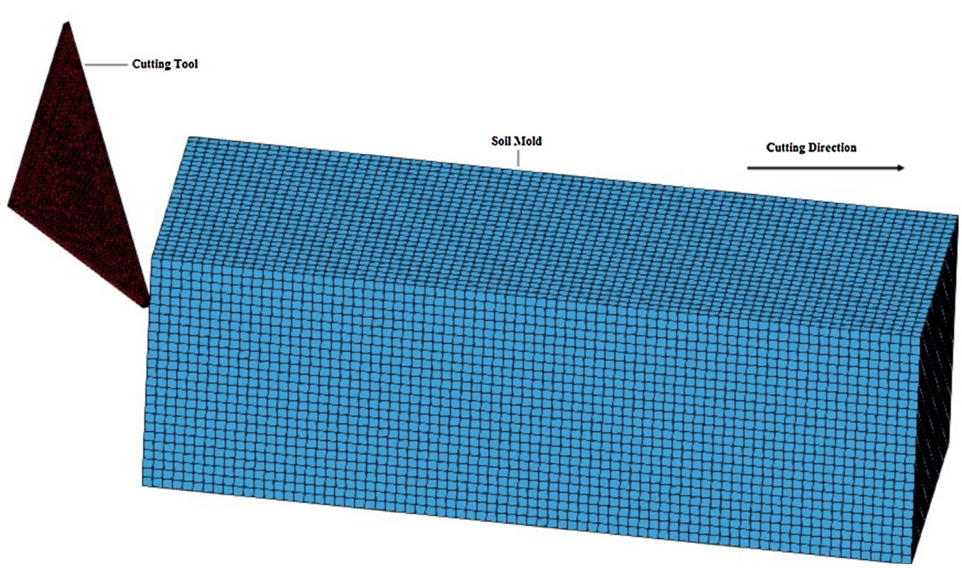

Fig. 1. Finite element meshing of soil and cutting tools before tool operation.

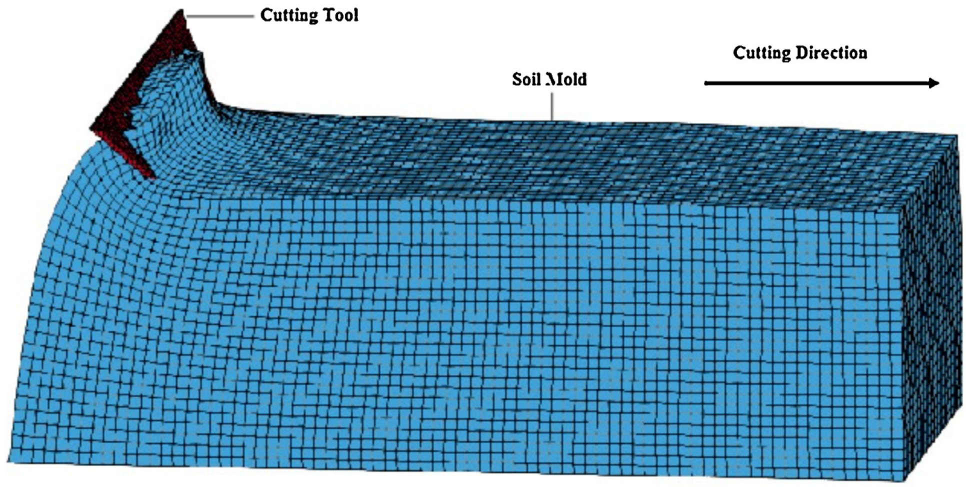

Fig. 2. Finite element meshing of soil and cutting tools before tool operation.

displacement. Moreover, Gee-Clough et al. (1994) modeled soil failure patterns in wet conditions (44% d.b.) using the finite element method. However, no information is currently available on the simulation of soil failure patterns observed at plastic consistency and liquid consistency limits, as well as at the sticky point of a soil. The objective of this study was therefore to investigate the use of FEM for the simulation of soil failure patterns as linked to consistency limits and the sticky point and to compare the simulation results with the soil failure patterns observed in the soil bin and in the field.

2. Materials and methods

The laboratory experiments were carried out in an indoor soil bin test rig developed at the Department of Agricultural Mechanization, College of Engineering, Nanjing Agricultural University (NJAU) (Tagar et al., 2014), while the field experiments were conducted at the Jiangpu Experimental Farm of Nanjing Agricultural University, Jiangsu Province, PRC, (lat. 32°3′4.96″N, long. 118°36′38.78″W). This region is generally hot and rainy in the summer and cold and dry in the winter, with an average annual temperature of 15.4 °C, an average annual precipitation of 1200 mm and a daily mean relative humidity of 76% (Li and Zhang, 2012). The top layer of soil (0–30 cm), which was used in the soil bin and field experiments, was composed of 50% sand, 24% clay and 26% silt and was classified as sandy clay loam. The bottom layer of soil (31–60 cm) comprised of 54% sand, 18% clay and 28% silt and was classified as sandy loam (yellow–brown soil according to the Chinese Soil Taxonomy, and Halpudalf according to the US classification scheme). This soil was used as paddy in a rice–wheat rotation on Nanjing Agricultural University's Jiangpu Experimental Farm. The soil plastic limit ($SMC_{pl,}$), liquid limit (SMC_{lq}), and sticky point (SMC_{sp}) were 32, 45 and 44%, respectively, while the organic carbon content of the soil was 9.6 g kg^{-1}.

2.1. Numerical simulation

2.1.1. Modeling and meshing

Three-dimensional finite element models were developed using the finite element software package Ansys/LS-Dyna explicit, version 13. Soil molds (300 mm × 100 mm × 100 mm) and cutting tool (150 mm × 120 mm × 4 mm) were drawn in Pro ENGINEER (Pro E) and then imported into Ansys/LS-Dyna. The material failure criterion was defined as eroding material. The convergence criterion was the L2 norm control convergence, and the convergence tolerance was 0.001 forces or moments. The soil was considered an isotropic material and the cutting tool was treated as a rigid body. Soil was modeled on the basis of the Drucker–Prager's elastic-perfectly plastic material law. The models were developed using 3D Solid Element 3D SOLID 164. The contact between the soil mold and cutting tool was made by surface to surface and eroding (ESTS). The meshing was done by MAPPED for the soil and SWEEP for the tool. Figs. 1 and 2 show finite element meshing of soil and tool models before and after tool operation. The size of soil model was approximately 26,026 elements and 29,484 nodes and that of the cutting tool model 1617 elements and 3400 nodes.

2.1.2. Boundary conditions and loading

As the model was symmetric, only one half of the soil and tool models were simulated in order to save computing time. The tool was modeled as a rigid body; therefore, all rotations' DOF (degrees of freedom) were constrained in the *x* and *y*-direction. The nodes of the soil in the underside plane were constrained in all DOF; the right plane was defined as a symmetry boundary plane. The other planes were left free, without any constraints, so that the soil particles could move in all directions. The tool was loaded with a velocity of 10 mm s^{-1} applied in the *z*-direction. The simulation time step was 0.2 s.

Table 1
The main material properties of soil models and cutting tool model.

Parameter		Moisture content (%)	Bulk density (Mg m^{-3})	Value	
				Elastic modulus (Pa)	Poisson's ratio
Soil model	Chip-forming failure	32	1.4	7.2×10^6	0.25
	Bending failure	32	1.4	8.1×10^6	0.27
	Flow failure	45	1.4	1.2×10^6	0.41
	Flow with considerable bending	44	1.3	1.35×10^6	0.39
Cutting tool model	–	–	–	7.56×10^6	0.3

Table 2
Other mechanical properties of soil used in the FEM simulation.

Property	Value
Specific gravity of soil used to obtain porosity, Spgrav	2.79
Density of water in model units, Rhowat	1.0000E-3
Viscoplasticity parameter, Vn	1.1
Viscoplasticity parameter, Gammar	0.0
Maximum number of plasticity iterations, Itermax	10
Initial bulk modulus or nonporous bulk modulus, K	1.260E+3
Shear modulus (non-zero), G	3.600E+2
Peak shear strength angle (friction angle) (radians), Phimax	1.436
Coefficient for modified Drucker–Prager surface, Ahyp	2.1600E-1
Eccentricity parameter for third invariant effects, Eccen	0.7
Strain hardening percent of peak shear strength angle, An	0.0
Strain hardening amount of nonlinear effects, Et	0.0
Parameter for pore-water effects on bulk modulus, Pwd1	0.0
Skeleton bulk modulus, pore-water parameter, PwKsk	0.0
Parameter for pore-water effects on effective pressure, Pwd2	0.0
Minimum internal friction angle (radians), Phires	0.0
Volumetric strain at initial damage threshold, Dint	3.6000E-7
Void formation energy, Vdfm	7.2000E+5
Level of damage that will cause element deletion (0.0–1.0), Damlev	0.99
Maximum principal failure strain, Epsmax	0.8

2.1.3. Soil and material properties

The input soil material properties, namely cohesion, friction, Young's modulus and Poisson's ratio, were measured with a standard triaxial compression apparatus. Young's modulus was calculated from the stress–strain ($\sigma_1 - \sigma 3$) curve at zero confining pressure or uniaxial compression ($\sigma_2 = \sigma_3 = 0$) obtained from the triaxial test using (Grote and Feldhusen, 2005):

$$E = \frac{100 \times \Delta(\sigma_1 - \sigma_3)}{\Delta\varepsilon} \tag{1}$$

where E is Young's modulus (kPa), $\Delta(\sigma_1 - \sigma_3)$ is the change in deviatoric pressure (kPa) and $\Delta\varepsilon$ is the change in elastic strain.

Poisson's ratio was calculated as (Grote and Feldhusen, 2005):

$$\nu = \frac{\varepsilon_{1R} - \varepsilon_{2R}}{\varepsilon_{1A} - \varepsilon_{2A}} \tag{2}$$

Where ε_{1R} is the initial thickness of the specimen before the test (mm), ε_{2R} is the thickness after the test (mm), ε_{1A} is the initial length of the specimen before the test (mm), and ε_{2A} is the length after the test (mm).

The values of dry bulk density for chip-forming failure, bending failure, flow failure and flow with considerable bending failure were obtained from experimental data. Soil–metal interaction properties were obtained from the modified direct shear box with a diameter of 61.0 mm and an area of 2920 mm^2. In this test, the lower half of the conventional direct shear box was replaced by a piece of the same metal used to manufacture the cutting tool, while soil was placed in the upper ring. The loads (12.5 N, 15.62 N and 21.82 N) were applied to the soil in the upper ring, whereas the bottom ring was moved horizontally. The shear strength properties were then determined based on the Mohr–Coulomb criterion. The material properties for the tool were obtained from MAT 147 (MAT_FHWA_SOIL) (Lewis, 2004), which obeys the modified Mohr–Coulomb yield criterion. The main soil and material properties are shown in Table 1 and other mechanical properties used in the FEM simulation are shown in Table 2.

2.2. Soil bin experiments

The soil molds were compacted to the ideal ρ_{dwb} (1.3–1.4 Mg m^{-3}) for sandy clay loam soil (USDA, 1999) and were then transferred to the soil bin in the soil cutting test rig. The cutting tool was then pushed through the soil mold at different

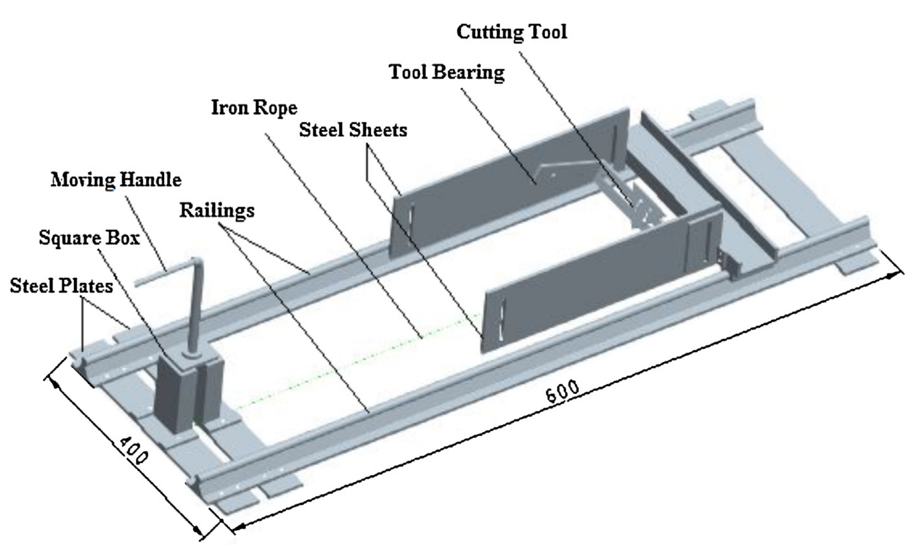

Fig. 3. Soil cutting test rig used in the field.

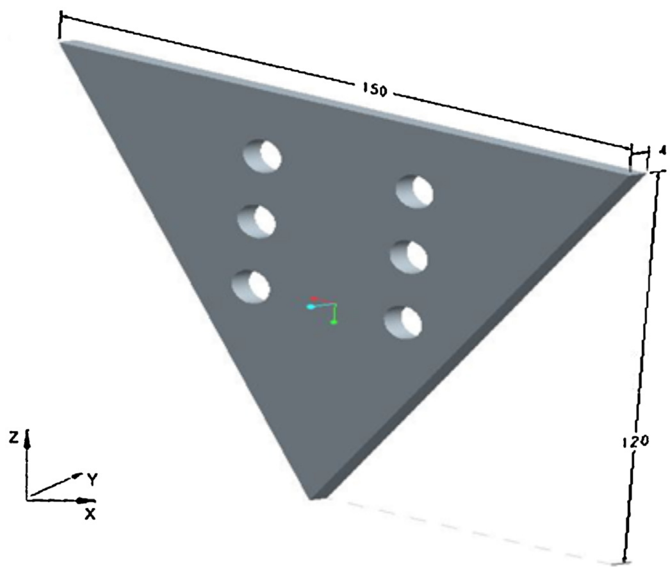

Fig. 4. Cutting tool used in the experiments.

angles in order to obtain the desired failure patterns. For a detailed description of soil preparation and the soil cutting test rig, the reader is referred to Tagar et al. (2014).

2.3. Field experiments

2.3.1. Preparation of test sites

Field conditions were quite heterogeneous (e.g., there were standing stubble and roots of preceding crops, and crop residues were present on the soil surface and mixed into the soil). To compare soil bin experiments with field experiments, the total field area was divided into five blocks (one without stubble and four with standing stubble (280 g m^{-2})). To create the stubble-free testing conditions, the preceding crop's stubble (rice crop (Wuyungen 23)) was removed using a lawn mower, though the roots remained. Under the standing stubble condition, both the stubble and roots were left undisturbed. Each of the blocks was then divided into subplots ($1.0 \times 1.0\,m^2$), to which the different types of failure patterns were then applied in a randomized design. Soil samples were taken from each subplot to determine the existing moisture content, and a calculated (Eq. (1)) amount of water was sprayed onto the subplots to bring the top 0.30 m of topsoil to the required consistency limits and sticky point. The field was then allowed to equilibrate to uniform moisture content for 20 h before the soil failure tests. Soil samples were taken from different locations of each subplot to ensure that the soil was evenly wetted.

2.3.2. Soil cutting test rig for the field

In order to mimic soil bin experiments at the field scale, a manually operated soil cutting test rig was developed. It consisted of a handle, iron cable, railings, and tool bearing and cutting tool (Fig. 3). Two railings, 600 mm long, were constructed in parallel, and were joined through steel plates (400 mm × 90 mm × 5 mm), two at the bottom and one at the head. The tool bearing along with cutting tool and steel sheets on the left and right sides were similar to those of the soil cutting test rig for the soil bin. These were mounted on the railings and joined by a steel plate (400 mm × 90 mm × 5 mm). A square box (100 mm × 50 mm) with a movable handle was fixed at the center of the steel plates. A cable rope (operated by hand), instead of a hydraulic system, was attached to the movable handle and tool bearing to pull the cutting tool in a forward direction to cut the soil, and in a backward direction to return it to the original position. For each cutting, the test rig was placed on the test site, and the handle was moved in a clockwise direction at the rate of 2 turns min^{-1} giving a speed of 10 mm s^{-1} to pull the tool carriage along with the cutting tool. As a result, the tool penetrated into the soil and cut the soil into different failure patterns.

2.4. Soil cutting procedure

The soil cutting test was performed at two consistency limits (SMC_{pl}, SMC_{lq}) and at the sticky point of soil (SMC_{sp}), factorially combined with three rake angles (15°, 30° and 45°) and three operating depths (30 mm, 50 mm and 70 mm)(Aluko and Seig, 2000; Makanga et al., 1997; Wang, 1991). A flat triangular shaped tool (150 mm long× 120 mm wide × 4 mm thick; Fig. 4), was used in both soil bin and field experiments. In order to adjust the cutting tool to different depths, two holes in each row, 20 mm apart, were drilled about 20 mm from the top at the center of the cutting tool. Videos were recorded to determine soil failure patterns using a

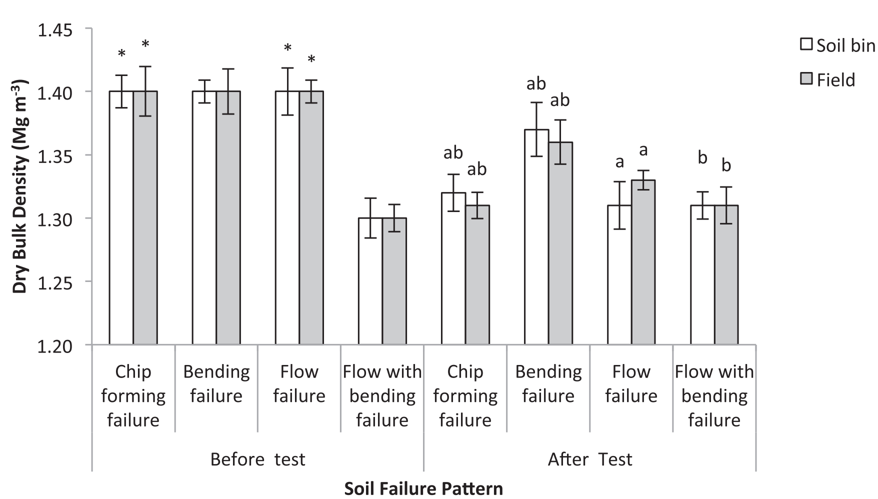

Fig. 5. Dry bulk density before and after different failure patterns in the soil bin and in the field. (Error bars represent standard error ($n = 4$). "Before test" bars marked with an asterisk (*) showed a significant difference as compared to the corresponding "after test" value. Different failure patterns within the same soil type (soil bin or field) with no letter in common in the "after test" section had significantly different impacts on the change in the soil properties).

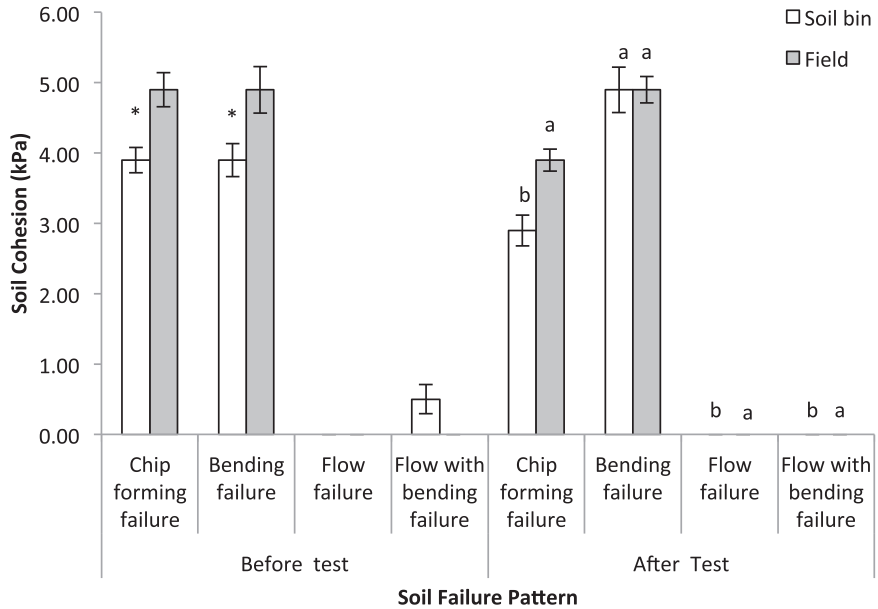

Fig. 6. Soil cohesion (no bar at zero soil cohesion) before and after different failure patterns in the soil bin and in the field. (Error bars represent standard error (n = 4). "Before test" bars marked with an asterisk (*) showed a significant difference as compared to the corresponding "after test" value. Different failure patterns within the same soil type (soil bin or field) with no letter in common in the "after test" section had significantly different impacts on the change in the soil properties).

digital camera (Canon Power Shot A4000 IS: 16 megapixels, Canon Inc. China). The recorded videos were converted to snapshots using a VLC media player (VLC, 2.0.2, Free Software Foundation, Inc. USA). Soil failure patterns were then identified as brittle failure when soil failed in the propagation of tensile cracks (Aluko and Seig, 2000), chip-forming failure when soil failed in the form of chips similar to the chips in metal cutting (Rajaram and Erbach, 1996; Rajaram and Gee-Clough, 1988), bending failure when soil was physically displaced with little strains of elements in the vertical direction (Elijah and Weber, 1971), flow failure when soil failed in a similar way to bending, but with no strains of elements (Elijah and Weber, 1971; Rajaram and Erbach, 1996; Rajaram and Gee-Clough, 1988), and flow with considerable bending failure when soil failed similar to flow failure but with considerable bending and no strains of elements (Tagar et al., 2014). Snapshots of soil failure patterns found in the soil bin, field and simulation were combined in joint figures. The chip-forming failure, bending failure, flow failure and flow with considerable bending failure patterns found in the soil bin tests were compared with the corresponding failure patterns observed in the field as well as with the simulated corresponding failure patterns. The soil structures produced after different failure patterns were also investigated in order to study the tilth condition of the soil.

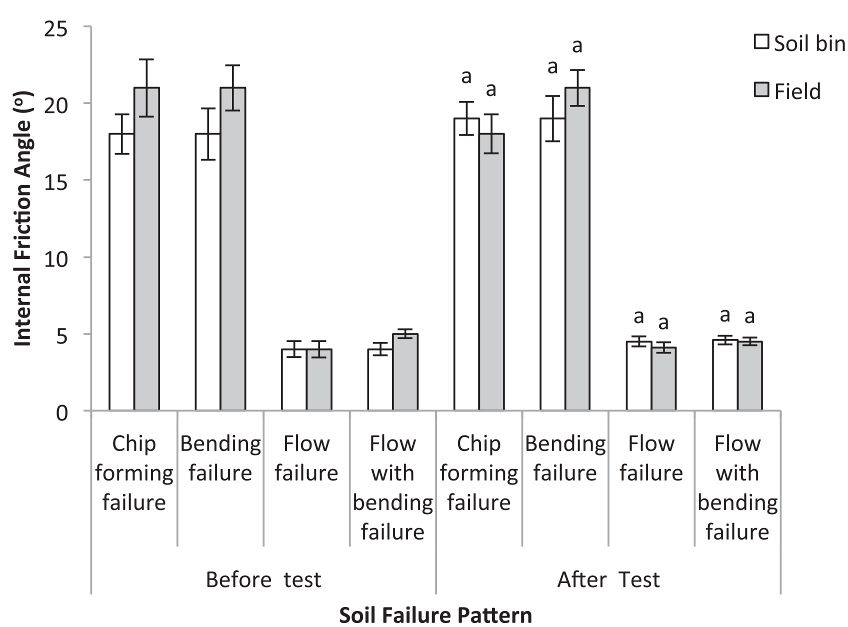

Fig. 7. Internal friction angle before and after different failure patterns in the soil bin and in the field. (Error bars represent standard error (n = 4). "Before test" bars marked with an asterisk (*) showed a significant difference as compared to the corresponding "after test" value. Different failure patterns within the same soil type (soil bin or field) with no letter in common in the "after test" section had significantly different impacts on the change in the soil properties).

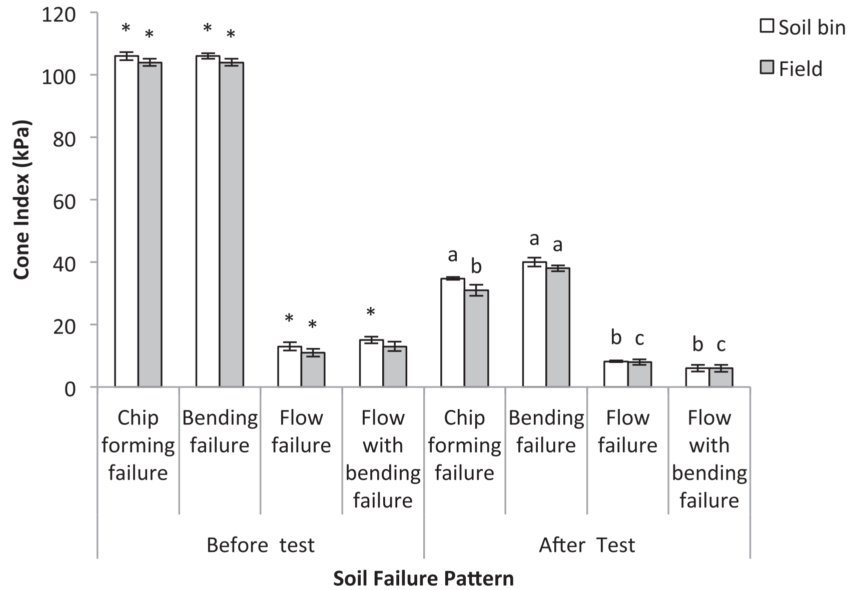

Fig. 8. Cone index before and after different failure patterns in the soil bin and in the field. (Error bars represent standard error ($n = 4$). "Before test" bars marked with an asterisk (*) showed a significant difference as compared to the corresponding "after test" value. Different failure patterns within the same soil type (soil bin or field) with no letter in common in the "after test" section had significantly different impacts on the change in the soil properties).

2.5. Soil physical and mechanical properties

Soil physical and mechanical properties may reveal quantitative information regarding the structure of a soil after different failure patterns. As outlined by a number of authors (e.g., Mamman and Oni, 2005; Rajaram and Erbach, 1996, 1997, 1998), it is indispensable to study the physical and mechanical properties of soil after different failure patterns in order to better understand the tilth condition of soil. To detect whether the structure of the soil after chip-forming failure, bending failure, flow failure and flow with considerable bending failure are suitable for good tilth conditions, soil physical (ρ_{dwb}) and mechanical (cohesion, internal friction angle and cone index) properties were measured. To measure the dry weight basis bulk density (ρ_{dwb}) of the soil molds in the soil bin as well as in the field, undisturbed soil core samples (50 mm diameter, 50 mm height) were collected at three different locations from both the soil molds in the soil bin and the test sites in the field. The mean ρ_{dwb} was then calculated using the

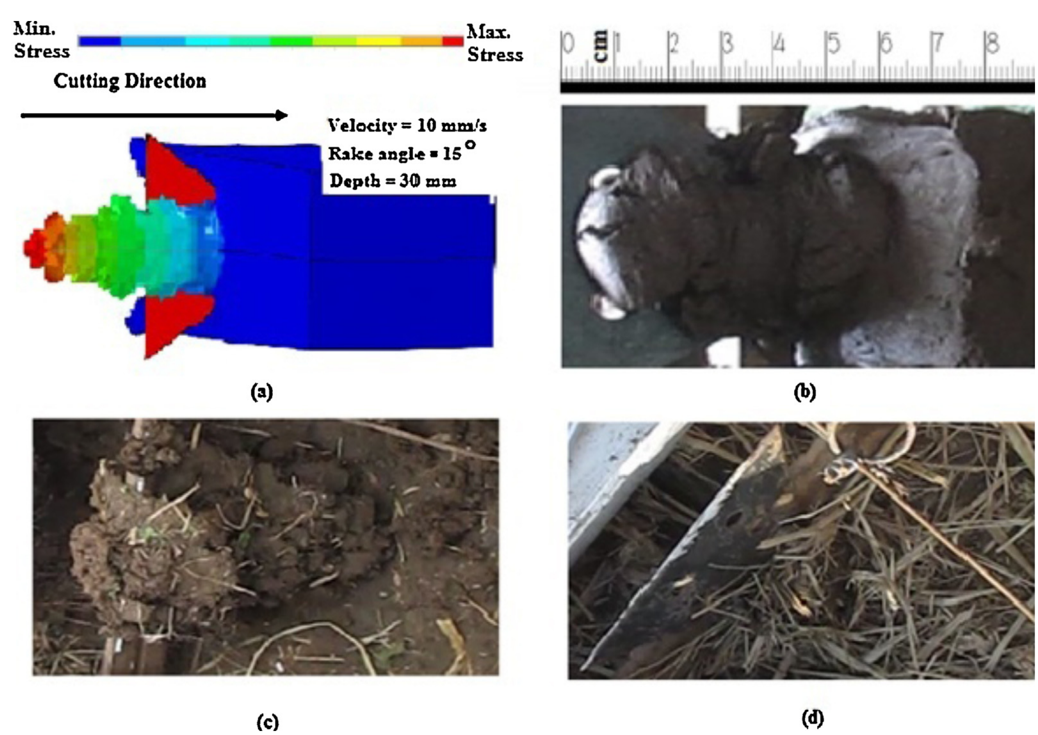

Fig. 9. Chip-forming failure pattern: (a) in the soil bin; (b) in the field (without stubble conditions); (c) in the field (with standing stubble conditions); (d) simulated chip-forming failure pattern.

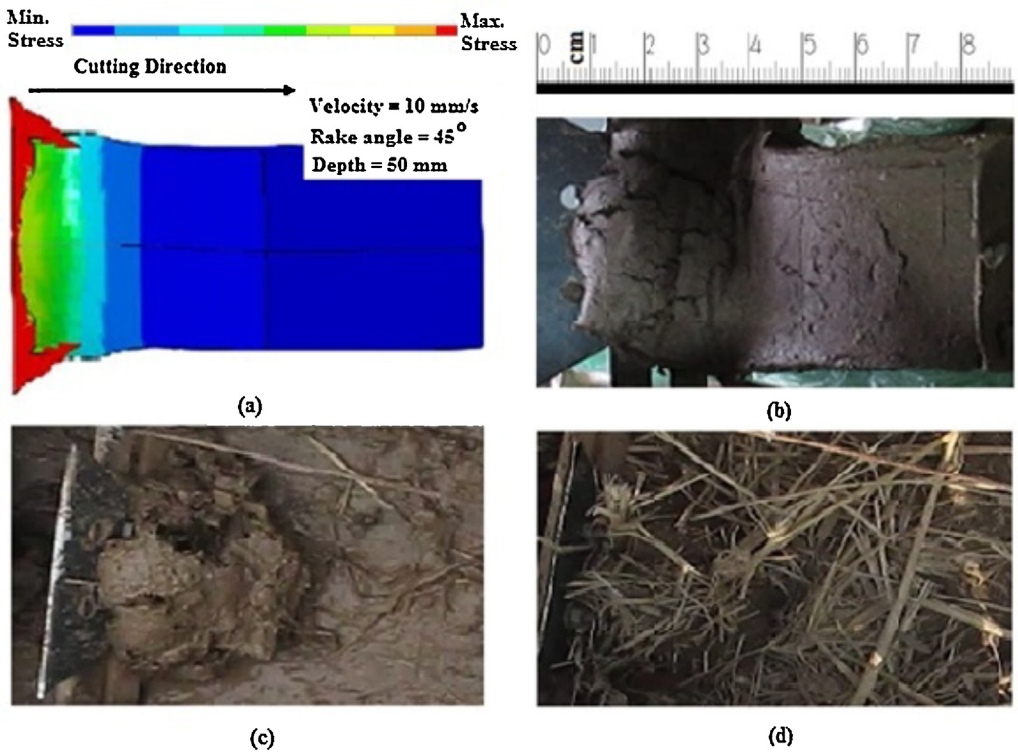

Fig. 10. Bending failure pattern: (a) in the soil bin; (b) in the field (without stubble conditions); (c) in the field (with standing stubble conditions); (d) simulated chip-forming failure pattern.

gravimetric method (Blake and Hartge, 1986). Soil textural class was determined by the hydrometer method (Bouyoucos, 1927). The soil plastic limit (SMC_{pl}) was determined as the gravimetric moisture content at which the soil just began to crumble as it was rolled into a thread of 3 mm in diameter (Sowers, 1965). To determine the soil liquid limit (SMC_{lq}), a 30° cone bearing a total weight of about 80 g was mounted on a shaft and allowed to rest on a cup (100 mL) full of soil for 5 s. The soil moisture content corresponding to a penetration of 20 mm on the linear relationship between soil moisture content (x-axis) and penetration (y-axis) was considered as the liquid limit (Campbell, 2001). The sticky point of soil (SMC_{sp}) was measured as the point at which the soil showed maximum stickiness/adhesion to the steel spatula (Baver, 1956). Organic carbon content (*SOCwb*) was determined using the Walkley and Black (1934) method.

2.6. Statistical analysis

Analysis of variance (ANOVA) was performed using the statistical software R (R Core Team, 2013) to evaluate the significance of the impact of different failure pattern treatments on the magnitude of the change in soil physical and mechanical properties ($n = 4$); differences between individual treatments were compared through pair wise t-tests using the Holm adjustment ($p = 0.05$). The significances of the changes in soil properties before and after specific tests, as well as the significance of differences in responses between soils, were analyzed through paired t-tests ($p = 0.05$).

3. Results and discussion

3.1. Soil physical and mechanical properties

The physical and mechanical properties of soil bin and field soils before and after different failure patterns are illustrated in Figs. 5–8. The soil cone index was significantly ($p < 0.05$) altered after all forms of failure in both soil and field conditions (with the exception of flow failure in field conditions). Soil bulk density was only significantly altered after chip-forming and flow failure, soil cohesion was only affected by chip-forming and flow failure in soil

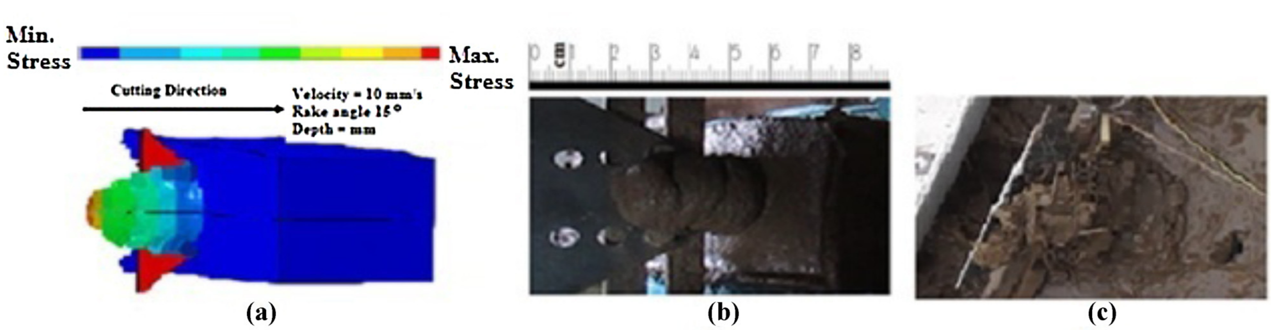

Fig. 11. Flow failure pattern: (a) in the soil bin; (b) in the field; (c) simulated flow failure pattern.

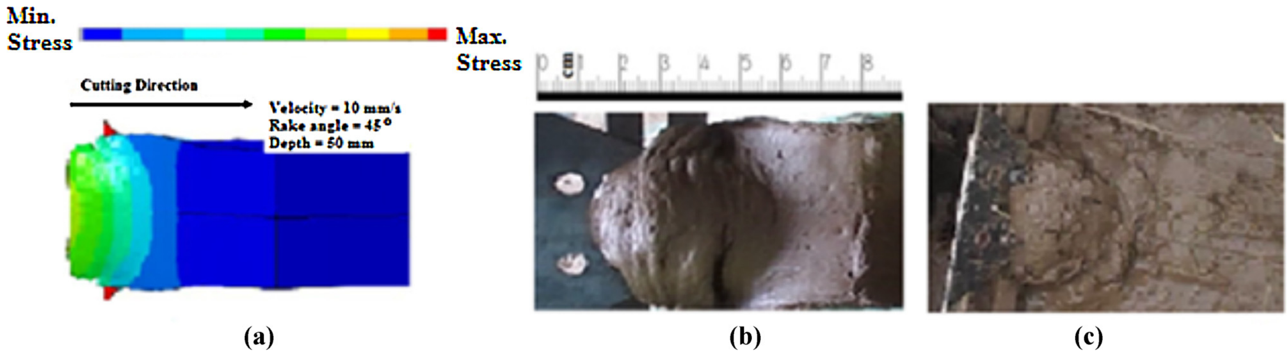

Fig. 12. Flow with bending failure pattern: (a) in the soil bin; (b) in the field; (c) simulated flow failure pattern.

bin conditions. On the other hand, the internal friction angle was not significantly altered in any of the tests. The ρ_{dwb} after (*vs.* before) chip-forming failure decreased from 1.4 to 1.32 Mg m^{-3} in the soil bin and from 1.4 to 1.31 Mg m^{-3}in the field. After (*vs.* before) flow failure pattern ρ_{dwb} decreased from 1.4 to 1.31 Mg m^{-3} in the soil bin and from 1.4 to 1.33 Mg m^{-3} in the field. However, changes in ρ_{dwb} for bending and flow with bending failure patterns were statistically non-significant (Fig. 5).

These results indicate that the ρ_{dwb} after different failure patterns was not conducive to good tilth. Generally, the growth of roots is limited by increasing soil bulk density and excessive soil resistance due to insufficient aeration or saturation by water (Greacen and Sands, 1980), and Masle and Passioura (1987) concluded that both high and low bulk densities can result in reduced crop establishment. Higher soil bulk density can reduce soil porosity, water holding capacity and root growth (Gebauer and Martinková, 2005). Tirado-Corbalá and Slater (2010) concluded that trees planted on sandy clay loam exhibited greatest dry root weight at the bulk density of 1.2 Mg m^{-3}, while bulk densities in the range of 1.4–2.2 Mg m^{-3} can limit the growth of roots (Patterson, 1977; Alberty et al., 1984; Randrup, 1998). An ideal soil contains about 50% solid particles and 50% pore space by volume (Hillel, 1982). As such, despite the decreases in bulk densities observed, none of the treatments reached ideal bulk density conditions.

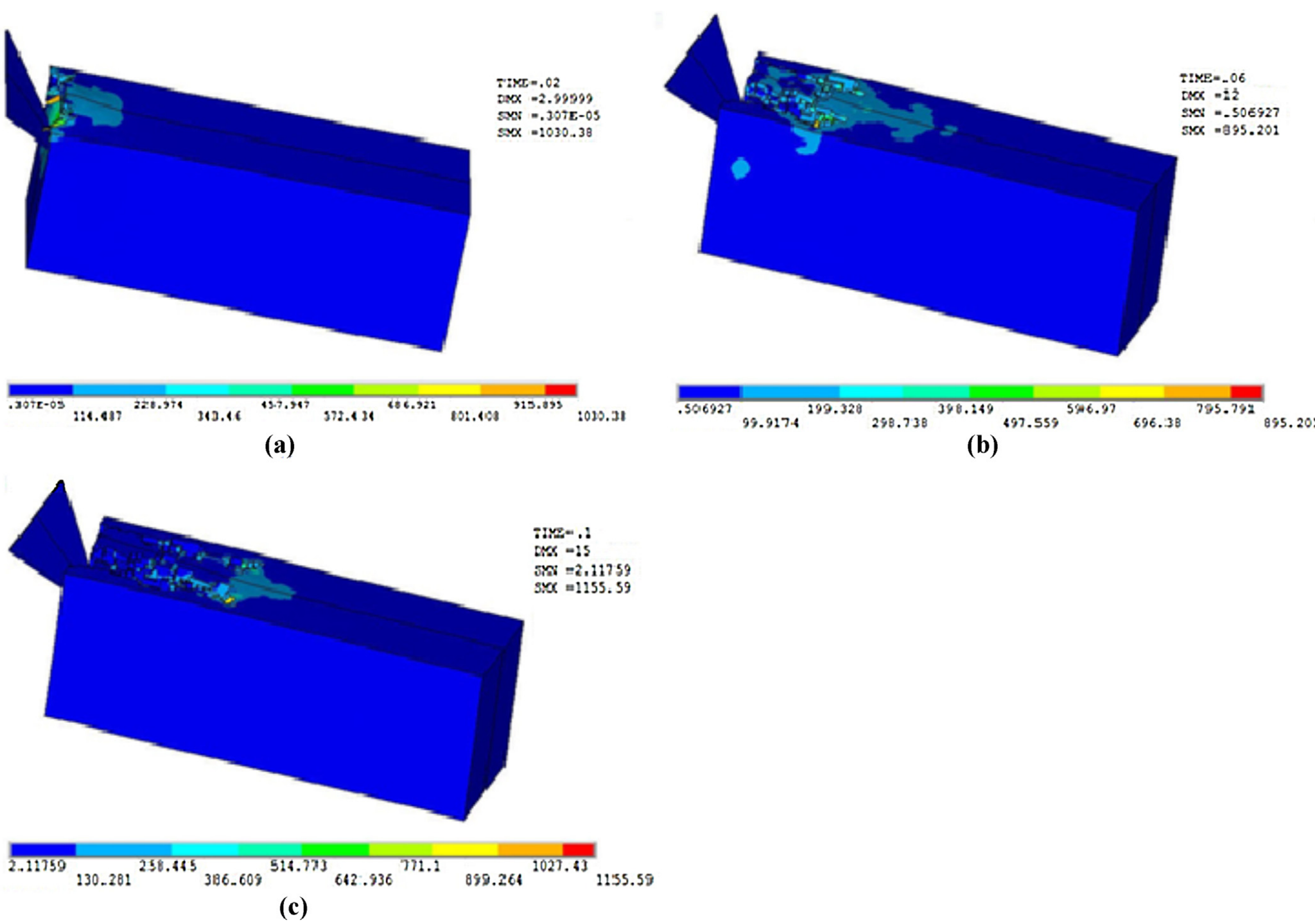

Fig. 13. Chip-forming failure: (a) stress at 0.02 s, (b) stress at 0.06 s and (c) stress at 0.1 s.

Soil cohesion slightly decreased between before and after chip-forming failure, from 3.9 to 2.9 kPa in the soil bin and from 4.9 to 3.9 kPa in the field. Soil cohesion increased slightly from 3.9 to 4.9 kPa in the soil bin after bending failure, but remained constant at 4.9 kPa in the field. Changes in soil cohesion after flow failure were negligible (Fig. 6). Changes in the internal friction angle, on the other hand, were statistically non-significant after all tests (Fig. 7).

The soil cone index decreased from 106 kPa to 34.78 kPa in the soil bin and from 104 kPa to 31 kPa in the field after chip-forming failure, and, after bending failure, from 106 kPa to 40 kPa in the soil bin and from 104 kPa to 38 kPa in the field. However, after flow failure pattern it decreased but slightly from 13 kPa to 8.22 kPa in the soil bin, while changes in the field were not significant. In the case of flow with considerable bending failure, the cone index also decreased significantly, though to a lesser extent: from 15 kPa to 6 kPa in the soil bin and from 13 kPa to 6 kPa in the field (Fig. 8).

The change in cohesion and internal friction angle were non-significant ($p > 0.05$) in soil bin and field tests for both chip-forming and bending failure, remaining constant or decreasing slightly after the former and increasing slightly after the latter. This may have occurred because, in chip-forming failure, the operating depth (30 mm) and rake angle (15°) were small, so that the soil failed in the form of chips, while in bending failure the operating depths (50 mm and 70 mm) and rake angles (30° and 45°) were large, so that the soil did not fail but rather molded. This is consistent with Keller and Dexter (2012), who mentioned that at the plastic limit, each soil particle is surrounded by a film of water that causes them to slide over each other, so that the soil therefore undergoes plastic deformation. However, those properties decreased significantly after flow failure and flow with considerable bending failure patterns in both soil bin and field tests. This is attributable that in flow failure and flow with considerable bending failure patterns, all pores are filled by water and the soil is capable of viscous flow (Keller and Dexter, 2012).

The soil cone index decreased significantly after nearly all types of soil failure patterns and conditions, potentially affecting soil workability. Shaw et al. (1942) and Busscher et al. (1997) concluded that soil moisture content is the dominant factor determining cone index, with lower moisture levels leading to increased cone indices, consistent with Henderson et al. (1988), who concluded that the cone index increased exponentially with the reductions in moisture content. According to Adeniran and Babatunde (2010), the high moisture content weakens soil molecular bonds, thereby decreasing the cohesive forces of the soil particles. This leads to cultivation practices becoming difficult, leading to high slippage, sinkage and smearing of machinery and loss of trafficability.

For efficient soil cultivation with a *SMC* beyond the critical value (23.72%), the soil needs to be drained before cultivation. Utomo and Dexter (1981) concluded that at high *SMC* levels, soils have relatively little strength and should not be considered suitable for tillage. This is supported by Bourma (1969), Kuipers (1982) and Keller and Dexter (2012) who concluded that if tillage is performed when soils are too wet (above the plastic limit), they lose their aggregate structure through the molding processes, creating unfavorable soil conditions. This is consistent with Dexter and Bird (2001) who concluded that when soil is tilled at a *SMC* exceeding the SMC_{pl}, the soil will deform plastically and thus lose its structure. Consequently, a soil with good workability usually has a SMC_{fc} that is lower than its SMC_{pl}

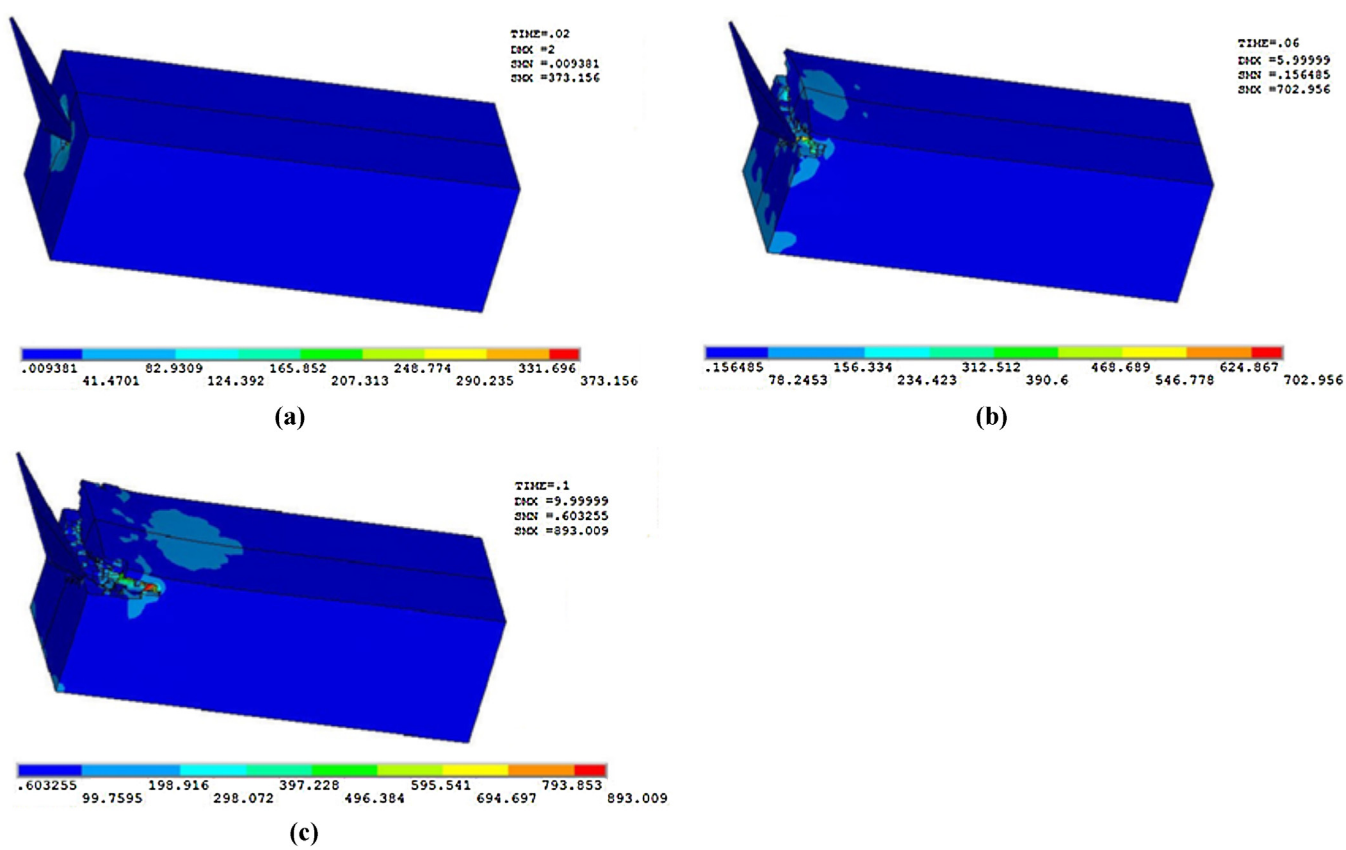

Fig. 14. Bending failure: (a) stress at 0.02 s, (b) stress at 0.06 s and (c) stress at 0.1 s.

(Barzegar et al., 2004; Keller and Dexter, 2012; Müller et al., 2003; Ojeniyi and Dexter, 1979; Utomo and Dexter, 1981; Watts and Dexter, 1998).

3.2. Comparison of simulated failure patterns with soil bin and the field

In the FEM simulation, the chip-forming failure pattern was observed at a 30 mm operating depth and 15° rake angle, as observed for both the soil bin and field tests at the plastic limit (Fig. 9a–c), with the size of the chips being equal to the operating width of the tine. In contrast, Rajaram (1987) and Rajaram and Erbach (1996) observed this type of failure at an *SMC* of 28.6% (slightly above the SMC_{pl}). Bending failure was observed at 50 mm and 70 mm depths of operation and 30° and 45° rake angles in the simulation, which matched that of the soil bin; however, the strains of elements seen with the soil bin were not present in the simulated failure pattern, while bending was not found in the field (Fig. 10a–c). This observation concurs with Elijah and Weber (1971), who found bending failure with little strains of elements at high moisture contents in a soil bin, but not in the field. Similar types of failure patterns were observed in the field with standing stubble conditions, but the failure patterns were found to be affected by the standing stubble and roots in the field (Figs. 9d and 10 d). The chip was 62 mm wide and 30 mm thick in the soil bin, while in the field the chip was 71 mm wide and 30 mm thick. However, the bending failure was 106 mm wide and 53 mm thick in the soil bin, while in the field the bending failure was 112 mm wide and 54 mm thick.

At the liquid limit, flow failure was observed at all operating depths (30 mm, 50 mm and 70 mm) and rake angles (15°, 30° and 45°) in the simulation, which closely followed that in the soil bin or field (Fig. 11a–c), although the roots of the stubble in the field did affect the soil flow failure pattern, giving it the appearance of chip-forming failure. Such a flow-type failure pattern was also observed by Wang (1991) at *SMC* levels of 44% and 52%, and by Rajaram and Gee-Clough (1988) at 42% in Bangkok clay soils. In contrast, Wang and Gee-Clough (1993) found brittle failure and shear failure patterns at 44% moisture content. However, our study found that flow failure is clearly related to the SMC_{lq} of the soil. Flow failure was 43 mm wide and 32 mm thick in the soil bin, while in the field it was 57 mm wide and 30 mm thick.

At SMC_{sp}, the flow with considerable bending as simulated for 50 mm and 70 mm operating depths and 30° and 45° rake angles closely matched that seen in the soil bin and to a lesser extent that seen in the field (Fig. 12a–c), where bending was slightly less than that observed in the soil bin. This difference may be due to the fact that, though the soil has a maximum stickiness at the sticky point of soil, it has a greater support and a larger cross-sectional area in the field (as in the case of soil bin). The flow failure (Makanga et al., 1996, 2010; Rajaram and Gee-Clough, 1988; Stafford, 1981; Wang, 1991) and bending failure patterns (Elijah and Weber, 1971) have already been explored in the literature; however, flow failure with considerable bending and no strains of elements at the sticky point has not been reported earlier. In the soil bin, the flow with considerable bending failure was 108 mm wide and 55 mm thick, while in the field the flow with bending failure was 105 mm wide and 51 mm thick.

Figs. 13–16 show that the minimum and maximum stresses in chip-forming, bending, flow and flow with bending failure patterns were highly variable with time, with maximum stresses of 1670 kPa at 0.02 s, 7150 kPa at 0.06 s and 7693 kPa at 0.1 s in the flow with bending failure pattern, while the minimum stresses were of 0.32 kPa at 0.02 s, 1.83 kPa at 0.06 s and 12.98 kPa at 0.1 s.

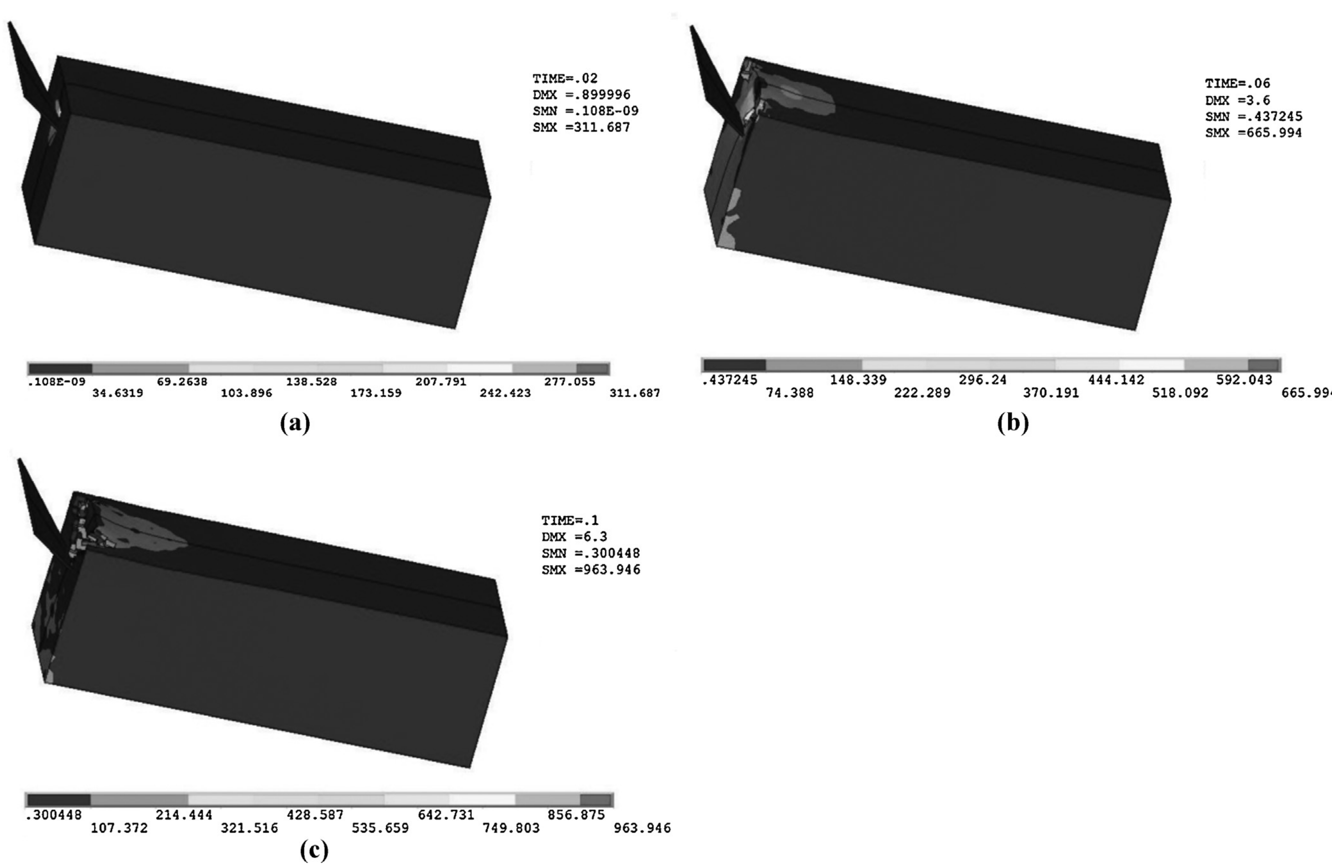

Fig. 15. Flow failure: (a) stress at 0.02 s, (b) stress at 0.06 s and (c) stress at 0.1 s.

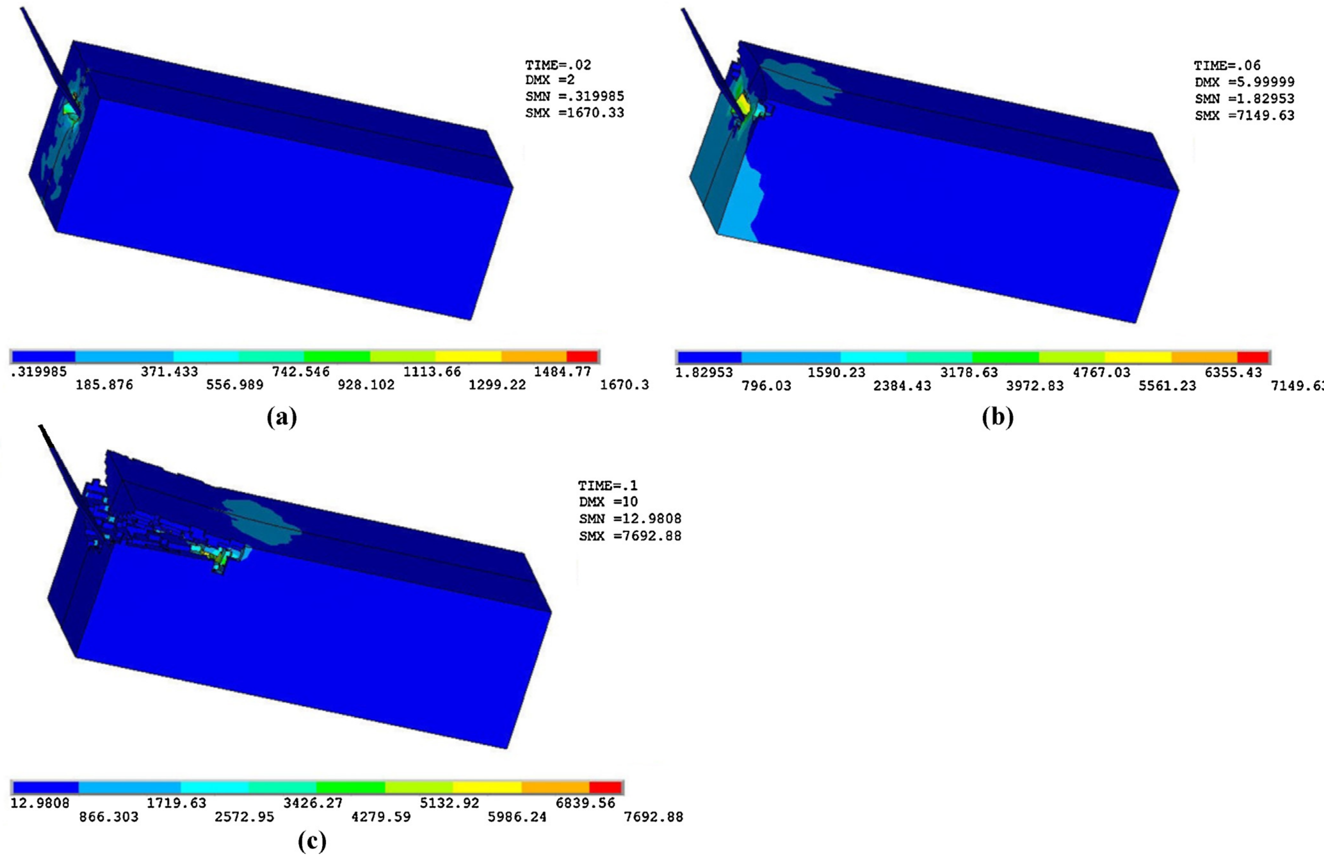

Fig. 16. Flow with bending failure: (a) stress at 0.02 s, (b) stress at 0.06 s and (c) stress at 0.1 s.

Thus, it is evident that the simulated chip-forming failure and flow failure patterns correlated well with the failure patterns found in the soil bin and in the field, while bending failure and flow with considerable bending failure correlated well with the soil bin only, because bending failure is not observed under field conditions at the plastic limit (field soil physical property tests for "bending failure" were obtained from failure at the same moisture content and rake angle and depth that caused bending failure in the soil bin). It is anticipated that if at the SMC_{pl} the operating parameters of the tool are small ($\leq$30 mm and $\leq$15°), then a smaller portion of the tool (30 mm) will enter and cut a lesser depth of soil in the form of chips without bending, because the remaining soil, having a larger cross-sectional area with respect to the operating parameters of tool, has more support. Comparatively, at the same SMC_{pl}, if the tool's operating parameters are large ($\geq$30 mm and $\geq$15°), a larger portion of the tool enters the soil, the tip of the tool cuts the soil, and the remaining part of the tool creates bending. However, in similar field conditions, though the operating parameters of the tool are large, the bending is not created, because the soil has a greater support and a larger cross-sectional area (resulting in chip-forming failure). The strains of elements in the vertical direction were larger and deeper in the field, possibly due to the roots of the stubble. However, slight bending was experienced at the SMC_{sp} of the soil. This is consistent with Gee-Clough et al. (1994), who conducted a study to investigate the use of FEM to predict wet clay soil response to a wide tine and concluded that the soil failure patterns were similar to those observed in soil bin experiments. It is evident that FEM provided good simulation of soil failure patterns; however, soil failure patterns correlated better with those found in soil bin tests as compared to the field tests in the presence of standing stubbles and their roots. This is consistent with Theuer (2011), who stated that in real field situations, a complex system of crop plants, clods, roots, and mixed terrain (soil mixed with stones etc.) renders the simulation more complicated, making it nearly impossible to account for all of these influencing factors. Karmakar and Kushwaha (2006) also confirm the limitation of FEM for dynamic effects in the simulation of soil–tool interactions. It is suggested that in future studies, other numerical methods (e.g., discrete element method and computational fluid dynamics) should also be explored for the more accurate simulation of field conditions.

4. Conclusions

In this study, the ability of FEM to simulate soil failure patterns at the plastic and liquid limits of soil in both laboratory (soil bin) and field conditions was evaluated. In general, FEM provided acceptable simulation of soil failure patterns; however, the simulation results correlated better with soil failure patterns found in soil bin tests as compared to the field tests in the presence of standing stubbles as well as their roots. This study has also shown that there is a direct relationship between soil failure patterns and the consistency limits of the soil both in the soil bin as well as in the field; however, bending failure was not properly observed in the field. Of the soil properties tested, only the soil cone index was consistently changed by all types of soil failure patterns; bulk density was only affected by chip and flow failure and soil cohesion was only affected by chip and bending failure in soil bin conditions, while the internal friction angle was not affected by any failure pattern in either soil bin or field conditions. This study has also shown that the soil structures produced after different failure patterns at the plastic and liquid limits of soils were not conducive to good tilth.

It is suggested that future research investigate the sticky consistency limit of soils, which occurs at lower moisture content compared to plastic limit and liquid limit as well as sticky point of soil, which may provide better soil physical conditions as compared to plastic and liquid consistency limits. Further investigation into the use of other numerical methods to accurately simulate soil failure patterns found in the field tests may also be of future interest.

Acknowledgements

This study was funded by the National Science Foundation of China (Grant Nos. 41371238; 51275250) and the Priority Academic Program Development of Jiangsu Higher Education Institutions (PAPD). Partial funding was also provided by an NSERC Discovery Grant, as well as a CFI grant, held by Jan Adamowski.

References

Abo Al-Kheer, A., Aoues, Y., Eid M., El-Hami, A., 2011.Integrating optimization and reliability tools into the design of agricultural machines. In: 20e Congre's Français de Me canique Besanç on, 29 aou t au 2 septembre 2011. AFM, Maison de la Me canique, Courbevoie, France. (accessed 29.04.2013) http://documents.irevues.inist.fr/bitstream/handle/2042/46919/cfm2011_327.pdf.
Abo Al-Kheer, A., Kharmanda, M.G., A. El Hami, A., Mouazen, A.M., 2011b. Estimating the variability of tillage forces on a chisel plough shank by modeling the variability of tillage system parameters. Comput. Electron. Agr. 78 (1), 61–70.
Adeniran, K.A., Babatunde, O.O., 2010. Investigation of wetland soil properties affecting optimum soil cultivation. J. Eng. Sci. Technol. Rev. 3 (1), 23–26.
Alberty, C.A., Pellet, H.M., Taylor, D.H., 1984. Characterization of soil compaction at construction sites and woody plant response. J. Environ. Hortic. 2, 48–53.
Aluko, O.B., 2008. Finite element aided brittle fracture force estimation during two-dimensional soil cutting. Int. Agrophys. 22, 5–15.
Aluko, O.B., Chandler, H.W., 2004. Characterization and modeling of brittle fracture in two dimensional soil cutting. Biosys. Engng. 88 (3), 369–381.
Aluko, O.B., Seig, D.A., 2000. An experimental investigation of the characteristics of and conditions for brittle failure in two-dimensional soil cutting. Soil Till. Res. 57 (3), 143–157.
Barnes, K.K., Bockhop, C.W., 1960. McLeod H E. Similitude studies of tillage implement forces. Agric. Eng. 41 (1), 32–37.
Barzegar, A.R., Hashemi, A.M., Herbert, S.J., Asoodar, M.A., 2004. Interactive effects of tillage system and soil water content on aggregate size distribution for seedbed preparation in Fluvisols in southwest Iran. Soil Till. Res. 78, 45–52.
Baver, L.D., 1956. Soil Physics. John Wiley & Sons, New York.
Blake, G.R., Hartge, k.H., 1986. Bulk density. In: Klute, A. (Ed.), Methods of Soil Analysis. Part 1. Physical and Mineralogical Methods. American Society of Agronomy and Soil Science Society of America, Madison, pp. 363–376.
Bourma, J., 1969. Micro-structure and stability of two sandy loam soils with different soil managements. Agricultural Research Report 724. Pudoc, Wageningen.
Bouyoucos, G.J., 1927. The hydrometer as a new method for the mechanical analysis of soils. Soil Sci. 23 (5), 343–353.
Busscher, W.J., Bauer, P.J., Camp, C.R., Sojka, R.E., 1997. Correction of cone index for soil water content differences in a coastal plain soil. Soil Till. Res. 43 (3–4), 205–217.
Campbell, D.J., 2001. Liquid and plastic limits. In: Smith, K.A., Mullins, C. (Eds.), Soil and Environmental Analysis: Physical Methods. Marcel Dekker, Inc., New York, pp. 349–376.
Chandler, H.W., 1984. The use of non-linear fracture mechanics to study the fracture properties of soils. J. Agric. Eng. Res. 29 (4), 321–327.
Chi, L., Kushwaha, R.L., 1987. Three-dimensional finite element analysis of soil failure under a narrow tillage tool. ASAE Paper No. 88-1582. St. Joseph, MI, USA.
Chi, L., Kushwaha, R.L., 1989. Finite element analysis of forces on a plane soil cutting blade. Can. Agric. Eng. 31, 135–140.
Coetzee, C.J., Els, D.N.J., 2009. Calibration of granular material parameters for DEM modelling and numerical verification by blade–granular material interaction. J. Terramechanics 46, 15–26.
Coleman, G.E., Perumpral, J.V., 1974. The finite element analysis of soil compaction. Trans. ASAE 17, 856–860.
Dexter, A., Bird, N.R.A., 2001. Methods for predicting the optimum and range of soil water contents for tillage based on the water retention curve. Soil Till. Res. 57 (4), 203–212.
Elijah, D.L., Weber, J.A., 1971. Soil failure and pressure patterns for flat cutting blades. Trans. ASAE 14 (4), 781–785.
Gebauer, R., Martinková, M., 2005. Effects of pressure on the root systems of Norway spruce plants (Piceaabies [L.] Karst). J. Forest Sci. 51, 268–275.
Gee-Clough, D., Wang, J., Kanok-Nukulchai, W., 1994. Deformation and failure in wet clay soil: part 3, finite element analysis of cutting of wet clay by tines. J. Agric. Eng. Res. 58 (2), 121–131.
Greacen, E.L., Sands, R., 1980. Compaction of forest soils: a review. Aust. J. Soil Res. 18, 163–189.
Grote, K.H., Feldhusen, J., 2005. Dubbel–Taschenbuch fur den maschinenbau, 21st ed. Springer, Berlin/Heidelberg.
Hatibu, N., 1987. The mechanical behaviour of brittle agricultural soils. Ph.D. Thesis. Department of Agricultural Engineering. University of Newcastle upon Tyne, Newcastle upon Tyne, UK.
Hemmat, A., Khorsandy, A., Shafaie, V., 2012. Soil failure mode in front of a multiple-tip horizontally operated penetrometer. Turk. J. Agric. For. 36 (2012), 476–485.
Henderson, C., Levett, A., Lisle, D., 1988. The effects of soil water content and bulk density on the compatibility and soil penetration resistance of some Western Australian sandy soils. Aust. J. Soil Res. 26 (2), 391–400.
Hillel, D., 1982. Introduction to Soil Physics. Academic Press, Inc., Orlando, FL, USA.
Jafari, R., TavakoliHashjin, T., Minaee, S., Raoufat, M.H., 2006. Large deformation modeling in soil?tillage tool interaction using advanced 3D nonlinear finite element approach. In: AM, Madureira (Eds.), Proc. 6th WSEAS Int. Conf. on Simulation, Modeling and Optimization, September 22–24, 2006. World Scientific and Engineering Academy and Society, Lisbon, Portugal, pp. 246–251.
Jayasuriya, H.P.W., Salokhe, V.M., 2001. A review of soil-tine models for a range of soil conditions. J Agric. Eng. Res. 79 (1), 1–13.
Karmakar, S., Kushwaha, R., 2006. Dynamic modeling of soil–tool interaction: an overview from a fluid flow perspective. J. Terramechanics 43, 411–425.
Keller, T., Dexter, A.R., 2012. Plastic limits of agricultural soils as functions of soil texture and organic matter content. Soil Res. 50 (1), 7–17.
Kuipers, H., 1982. Processes in soil physical degradation in mechanized agriculture. In: Boels, C.D., Davies, B.D., Johnston, A.E. (Eds.), Soil Degradation. Galkema, Rotterdam.
Lewis, B.A., 2004. Evaluation of LS-DYNA Soil Material Model 147. Report No. FHWA-HRT-04-094. Federal Highway Administration.
Li, M., Zhang, H., 2012. Hydrophobicity and carbonation treatment of earthen monuments in humid weather condition. Sci. China Tech. Sci. 55 (8), 2313–2320.
Liu-Yan, HouZhi-Min 1985. Three dimensional nonlinear finite element analysis of soil cutting by narrow blades. Proc. Int. Conf. Soil Dynamics, Auburn, AL, USA, 2, 322-337.
Liu, J., Chen, Y., Lobb, D.A., Kushwaha, R.L., 2007. Soil-straw-tillage tool interaction: field and soil bin study. Can. Biosyst. Eng. 49, 2.1–2.6.
Makanga, J.T., Salokhe, V.M., Gee-Clough, D., 1996. Effect of tine rake angle and aspect ratio on soil failure patterns in dry loam soil. J. Terramechanics 33 (5), 233–252.
Makanga, J.T., Salokhe, V.M., Gee-Clough, D., 1997. Effect of tine rake angle and aspect ratio on soil reactions in dry loam soil. J. Terramechanics 34 (4), 235–250.
Makanga, J.T., Salokhe, V.M., Gee-Clough, D., 2010. Deformation and force characteristics caused by inclined tines in loam soil with moisture content below liquid limit. J. Agric. Sci. Technol. 12 (2), 181–205.
Mamman, E., Oni K.C., 2005. Draught performance of range of model chisel furrowers. CIGR Ejournal.PM 05 003. 7, 1–17. http://hdl.handle.net/1813/10474 (accessed 3.07.13.).
Masle, J., Passioura, J.B., 1987. The effect of soil strength on the growth of young wheat plants. Aust. J. Plant Physiol. 14, 643–656.
McKyes, E., Desir, F.L., 1984. Prediction and field measurement of tillage tool draft forces and efficiency in cohesive soils. Soil Till. Res. 4 (4), 459–470.
Müller, L., Schindler, U., Fausey, N.R., Lal, R., 2003. Comparison of methods for estimating maximum soil water content for optimum workability. Soil Till. Res. 72 (1), 9–20.
Ojeniyi, S.O., Dexter, A.R., 1979. Soil factors affecting the macrostructures produced by tillage. Trans. Am. Soc. Agric. Eng. 22, 339–343.
Patterson, J., 1977. Soil compaction-effects on urban vegetation. J. Arboric. 3, 161–167.
R Core Team, 2013. R: A language and environment for statistical computing. R Foundation for Statistical Computing, Vienna, Austria. http://www.R-project.org/.
Rajaram, G., 1987. Force-time behavior of tine implements. M. Eng. Thesis No. AE -87-14. Asian Institute of Technology, Bangkok, Thailand.
Rajaram, G., 1990. Collapse failure in dry clay soils caused by tine implements. J. Terramechanics 27 (2), 6–78.
Rajaram, G., Erbach, D.C., 1996. Soil failure by shear versus soil modification by tillage: a review. J. Terramechanics 33 (6), 265–272.
Rajaram, G., Erbach, D.C., 1997. Hysteresis in soil mechanical behavior. J. Terramechanics 34 (4), 251–259.
Rajaram, G., Erbach, D.C., 1998. Drying stress effect on mechanical behavior of a clay-loam soil. Soil Till. Res. 49 (1–2), 147–158.
Rajaram, G., Erbach, D.C., 1999. Effect of wetting and drying on soil physical properties. J. Terramechanics 36 (1), 39–49.
Rajaram, G., Gee-Clough, D., 1988. Force–distance behavior of tine implements. J. Agric. Eng. Res. 41 (2), 81–98.
Randrup, T.B., 1998. Soil compaction on construction sites. In: Neely, D., Watson, G. W. (Eds.), The landscape below ground II: Proceedings of an International Workshop on Tree Root Development in Urban Soils. International Society of Arboriculture, Champaign, IL, pp. 146–153.
Raper, R.L., Erbach, D.C., 1990. Prediction of soil stresses using the finite element method. Trans. ASAE 33 (3), 725–730.

Shahab Davoudi, Reza Alimardani, Alireza Keyhani, Reza Atarnejad, 2008. A two dimensional finite element analysis of a plane tillage tool in soil using a non-linear elasto-plastic model. Amer-Eurasian J. Agric. Environ. Sci. 3 (3), 498–505.

Shaw, Haise, H.R., Farnsworth, R.B., 1942. Four years' experience with a soil penetrometer. Soil Sci. Soc. Am. Proc. 7, 48–55.

Shmulevich, I., 2010. State of the art modeling of soil–tillage interaction using discrete element method. Soil Till. Res. 111, 41–53.

Sowers, G.F., 1965. ConsistencyIn: Black, C.A., Evan, D.D., White, J.L., Ensimenger, L.E., Clark, F.E. (Eds.), Methods of Soil Analysis (Part 1), Physical and Mineralogical Properties, Including Statistics of Measurements and Sampling Agronomy Monograph 9. American Society of Agronomy, Madison, pp. 391–399. . c31 http://dx.doi.org/10.2134/agronmonogr9.1.

Stafford, J.V., 1979a. The performance of a rigid tine in relation to soil properties and speed. J. Agric. Eng. Res. 24 (1), 41–56.

Stafford, J.V., 1979b. A versatile high-speed soil tank for studying soil and implement interaction. J. Agric. Eng. Res. 24, 57–66.

Stafford, J.V., 1981. An application of critical state soil mechanics. The performance of rigid tines. J. Agric. Eng. Res. 26 (5), 387–401.

Tagar, A.A., Ji Changing, Ding Qishuo, Jan Adamowski, Chandio, F.A., Mari, I.A., 2014. Soil failure patterns and draft as influenced by consistency limits: an evaluation of the remolded soil cutting test. Soil Till. Res. 137, 58–66.

Theuer, J., 2011. Finite element modelling of the interaction between flexible tines and soil for mechanical weeding. Thesis submitted in the partial fulfilment of the requirements for the degree of MSc by Research. Cranfield University. https://dspace.lib.cranfield.ac.uk/bitstream/1826/7307/1/Jan_Theuer_Thesis_2011.pdf.

Tirado-Corbalá, R., Slater, B.K., 2010. Soil compaction effects on the establishment of three tropical tree species. Arboric. Urb. Forest. 36 (4), 164–170.

USDA, 1999. Soil Quality Test Kit Guide. USDA Soil Quality Institute, Washington, D. C.

Utomo, W.H., Dexter, A.R., 1981. Effect of ageing on compression resistance and water stability of soil aggregates disturbed by tillage. Soil Till. Res. 1, 127–137.

Walkley, A., Black, I.A., 1934. An examination of the Degtjareff method for determining organic carbon in soils: effect of variations in digestion conditions and of inorganic soil constituents. Soil Sci. 63, 251–263.

Wang, J., 1991. Stress-strain relationship in wet clay soil and some applications. AIT D. Eng. Dissertation No. AE -91-1. Asian Institute of Technology, Bangkok, Thailand.

Wang, J., Gee-Clough, D., 1993. Deformation and failure in wet clay soil, Part 2: soil bin experiments. J. Agric. Engg. Res. 54 (1), 57–66.

Watts, C.W., Dexter, A.R., 1998. Soil friability: theory, measurement and the effects of management and organic carbon content. Eur. J. Soil Sci. 49, 73–84.

Wegscheid, E.L., Myers, H.A., 1967. Soil bin instrumentation. Agric. Eng. 48 (8), 442–445.

Yong, R.N., Hanna, A.W., 1977. Finite element analysis of plane soil cutting. J. Terramechanics 14 (3), 103–125.